ADVANCED FUNCTIONAL MATERIALS
www.afm-journal.de

Reversible Electrochemically Triggered Delamination Blistering of Hydrogel Films on Micropatterned Electrodes

Ben B. Xu, Qihan Liu, Zhigang Suo, and Ryan C. Hayward**

Stimuli responsive elastic instabilities provide opportunities for controlling the structures and properties of polymer surfaces, offering a range of potential applications. Here, a surface actuator based on a temperature and electrically responsive poly(*N*-isopropyl acrylamide-co-sodium acrylate) hydrogel that undergoes a two-step delamination and buckling instability triggered using micropatterned electrodes is described. The electrically actuated structures entail large out-of-plane displacements that take place on time-scales of less than 1 s, in response to modest triggering voltages (–3–6 V). Alongside these experimental observations, finite element simulations are conducted to better understand the two-step nature of the instability. In the first step, hydrogel films undergo delamination and formation of blisters, facilitated by electrochemical reduction of the thiol groups anchoring the film to the electrodes. Subsequently, at larger reducing potentials, the electrolytic current is sufficient to nucleate a gas bubble between the electrode and the gel, causing the delaminated region to adopt a straight-sided blister shape. Finally, thermally induced deswelling of the gel allows the film to be returned to its flat state and readhered to the electrode, thereby allowing for repeated actuation.

1. Introduction

Elastic buckling instabilities of thin polymer films including wrinkling, creasing, folding, and global buckling modes provide both a rich set of fundamental questions in elasticity and a variety of potential applications.[1–5] From the latter perspective, buckled thin film structures have been integrated into devices to prevent failure under large deformations,[6–8] provide mechanically gated electrical switches,[9] improve the efficiency of organic solar cells,[10] regulate transport in microfluidic channels,[11,12] and tune the chemistry,[13] adhesion,[14,15] wetting,[16,17] and optical characteristics[18] of surfaces, among other examples.

In comparison to other buckling modes, delamination—wherein a supported elastic thin film subject to a compressive mismatch strain undergoes debonding from the substrate and forms blister-like structures—has received relatively little attention with regards to applications in responsive materials or soft actuators. Although well-known from the perspective of failure of a diversity of thin coatings including paint, metals and inorganic materials,[19,20] graphene[21–25] and polymer films,[26–32] and of recent interest in the growth of biofilms,[33–35] only a few studies have sought to exercise control over this process to define switchable materials. Notably, Huck and co-workers demonstrated the triggered electrochemical delamination of cross-linked polymer brush films from patterned electrodes, although in this case the process was irreversible.[36] Very recently, Rogers and co-workers have relied on delamination buckling of metal films with patterned adhesion to generate reversibly tunable 3D structures,[37] while Zhao and co-workers have used delamination of graphene films to tune surface wetting and transparency.[38]

Desirable materials for the fabrication of soft actuators should allow for large-scale, rapid, and reversible deformations. Polyelectrolyte gels have received considerable attention in this regard,[39,40] as they can reversibly undergo pronounced changes in shape or size in response to a wide range of stimuli[26,40–43] including changes in pH, ionic strength, temperature, light intensity, solvent composition, and electric or magnetic field strength. The electrically responsive characteristics of these materials are particularly attractive with regards to integration into microfabricated electrical control systems.[44,45] For example, Park and co-workers recently described a nanostructured polyelectrolyte electroactuator consisting of sulphonated block copolymers and ionic liquids,[46] which allowed for rapid response rates (<1 s), reasonably large strains (up to 4%), and reproducible actuation at below 1 V. Similarly, some of us previously reported that the application of modest voltages (2–4 V) to thin polyelectrolyte hydrogel layers allowed for rapid (≈1 s) actuation of surface creases.[47]

In the current report, we describe the reversible electrically actuated delamination and buckling of a thermally responsive

Dr. B. B. Xu, Prof. R. C. Hayward
Polymer Science and Engineering Department
University of Massachusetts
Amherst, 01003 MA, USA
E-mail: hayward@umass.edu
Dr. B. B. Xu
Smart Materials and Surfaces Lab
Faculty of Engineering and Environment
Northumbria University
Newcastle upon Tyne NE1 8st, UK
Q. Liu, Prof. Z. Suo
School of Engineering and Applied Sciences
Kavli Institute for Nanobio Science and Technology
Harvard University
Cambridge, 02138 MA, USA
E-mail: suo@seas.harvard.edu

DOI: 10.1002/adfm.201504769

poly(*N*-isopropylacrylamide-*co*-sodium acrylate) (PNIPAM) polyelectrolyte gel layer on micropatterned electrode surfaces. Through a two-step mechanism corresponding to electrochemically triggered delamination at a first critical voltage, followed by gas bubble formation at a second critical voltage, we demonstrate that large out-of-plane displacements can be achieved, with rapid switching at modest triggering voltages (from −3 to −6 V). Using thermally triggered deswelling of the gel, we show that it is possible to return the gel to its initially flat and adherent state, enabling reproducible formation of buckled structures through multiple cycles of actuation.

2. Results and Discussion

We consider the electrically triggered delamination and buckling of anionic PNIPAM copolymer gel surfaces supported on silicon substrates micropatterned with gold interdigitated electrodes (IDE) with widths w, spaced by an edge-to-edge distance a, as illustrated in **Figure 1**. A silane coating is used to maintain adhesion of the gel to the regions of the surface not covered by electrodes (without which, the gel is subject to extensive delamination upon swelling; see Figure S1a in the Supporting Information), while a thiol monolayer provides an electrochemically switchable bonding of the gel to the gold microelectrodes.[48–51] We also find that the thiol monolayer reduces the formation of bubbles due to electrolysis of water (Figure S1b, Supporting Information). The well-known thermal sensitivity of PNIPAM gels,[52,53] which undergo deswelling as temperature is increased, provides a simple means to modulate the compressive mismatch strain within the surface-attached gel, and therefore the elastic driving force for delamination and buckling. The gel is maintained in a phosphate buffered saline (PBS) solution (ionic strength = 150×10^{-3} M) and initially allowed to reach swelling equilibrium at a fixed temperature prior to electrical actuation. We characterize the degree of swelling in the gel by the ratio of the swelled thickness H, to the initial, as-prepared thickness h.

Upon increasing the DC electrical potential (Φ) applied between the anode and cathode lines in the IDE array, we observe a two-step electrochemical delamination and buckling process, as detailed in **Figure 2** for the case of h = 25 μm, w = 60 μm, and a = 120 μm (see also Movie S1 in the Supporting Information). Over the anode regions, we see the development of creases and craters as explored in a previous report,[47] which we will not consider further here. Over the cathodes, the gel thickness increases slightly due to electrochemically induced modulation of the swelling.[54,55] We quantify this behavior by plotting A/H (Figure 2g), with A representing the maximum vertical distance between the top surface of the gel and the underlying substrate, which reveals a slow increase in thickness starting at an applied potential of around −2 V. At a first critical voltage (around −4 V), the gel can be seen to delaminate from the cathode and buckle out-of-plane through a process of localized nucleation and rapid lateral propagation of blisters over a distance of at least 0.75 mm within 1 s. Interestingly, cross-sectional imaging of the film by laser-scanning confocal fluorescence microscopy (LSCM) reveals only a very small gap between the electrode surface and the gel, along with a clear region where the delaminated bottom surface of the gel exhibits self-contact. Once the gel has undergone delamination, the buckled features remain in place after turning off the applied potential, at least over a time-scale of 6 h. These 'stage I' blisters also exhibit secondary buckling along the direction of the electrodes, which take irregular morphologies under some conditions (Figure 2b), and periodic 'telephone-cord' structures under others (Figure 2e). We will discuss these features in more detail below, and note that similar observations (self-contact and telephone-cord morphologies) were reported by Velankar and co-workers[28] for swelling induced delamination of cross-linked polymer films.

Further increases in applied potential do not noticeably influence the delamination blisters, until a second critical voltage where the buckled gel inflates into a straight-sided blister, often referred to as an "Euler column".[31,56,57] These features also appear by localized nucleation and rapid lateral propagation with speeds up to 1.5 mm s^{-1} along the electrode, and yield quite pronounced contrast in bright-field optical microscopy, suggesting a large refractive index difference. Imaging by LSCM (Figure 2e,f) reveals a shape that is nearly a cosine in cross-section with a large gap between the bottom gel surface and the electrode. These features remain stable after turning off the applied voltage over times of at least 1 h, and do not revert to either stage I blisters or planar surfaces.

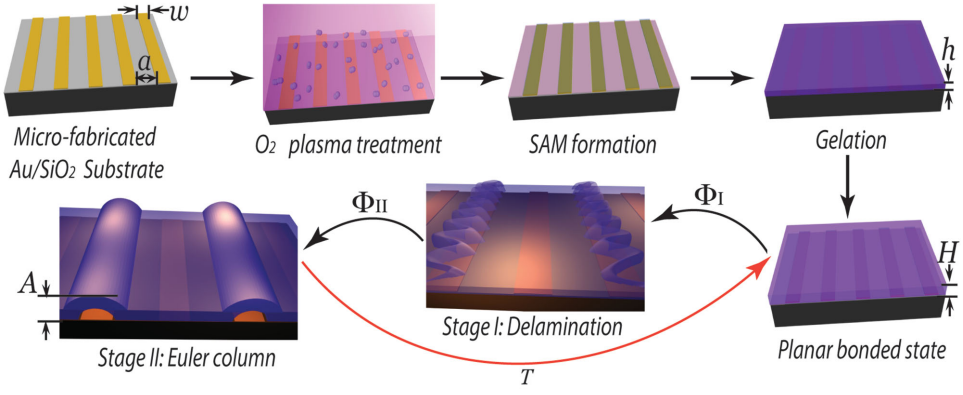

Figure 1. Microfabrication and actuation of gel films. Schematic illustration of the fabrication and actuation of a responsive gel-based film supported on an interdigitated electrode array. The gel film is preswelled to a level H/h in the vertical direction in PBS solution prior to electrochemical actuation.

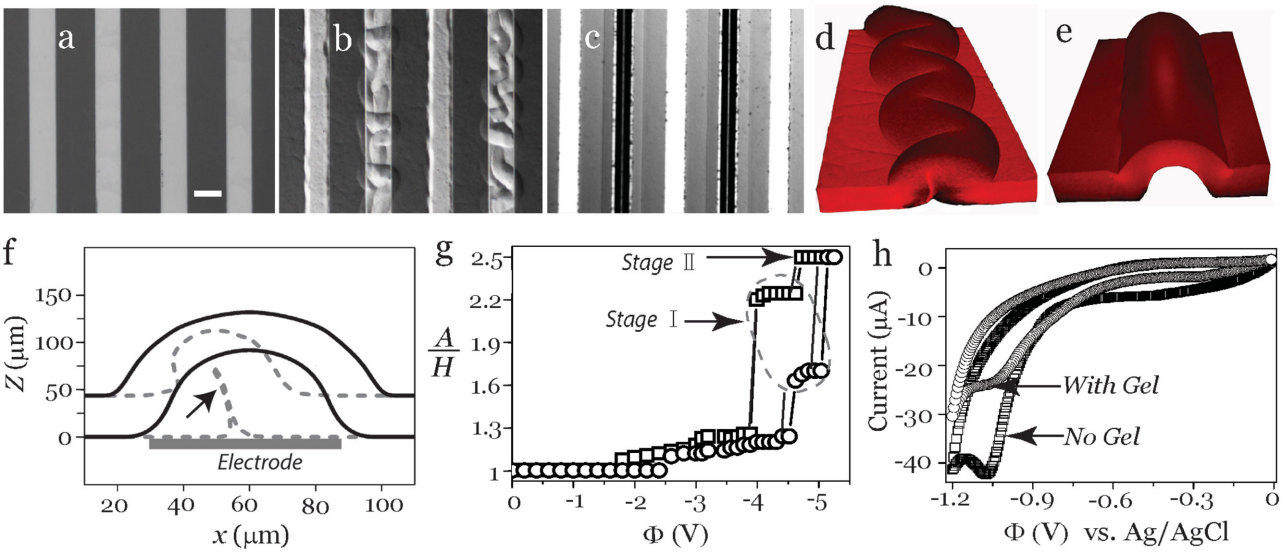

Figure 2. Experimental characterization of two-stage delamination buckling. a) While the surface is initially flat, increasing the applied potential results in b) stage |—delamination and buckling, followed by c) stage ‖—formation of a straight-sided 'Euler column'. The scale bar is 50 μm. LSCM 3D reconstructed images show d) a stage | delamination exhibiting a regular 'telephone cord' morphology, and e) a stage ‖ Euler column. f) Cross-sectional profiles extracted from the LSCM images are compared for stage I (dotted line) and stage II (solid line), with the self-contacting region indicated by the arrow. g) The stepwise actuation is shown by plotting the normalized out-of-plane displacement of gel (A/H) as a function of the applied voltage at two different swelling ratios, $H/h = 1.9$ (squares), and $H/h = 1.5$ (circles), ($h = 25$ μm, $w = 60$ μm, $a/w = 2$). h) Cyclic voltammetry measurements show the reduction of the thiol—Au bond at −1.02 V.

We first consider the electrochemical and mechanical phenomena underlying this two-step delamination process. Stage I delamination is triggered by reductive desorption of the thiol monolayer at the cathode, a process also employed by Huck and co-workers for electrically triggered debonding of thin films.[36] Cyclic voltammetry (CV) measurements (Figure 2h) reveal that this process occurs at −1.02 V, relative to Ag/AgCl, for a homogeneous planar gold electrode covered with a self-assembled monolayer of the thiol used here, and that this value is insensitive to the presence of a hydrogel coating. The value also agrees well with those from previous reports.[50,51] This value cannot be directly compared to the critical potentials necessary to trigger stage I delamination in the IDE geometry, as the potential drop at each electrode is unknown, although a sudden increase in electrochemical current between the micropatterned electrodes (Figure S2, Supporting Information) at a voltage similar to that required for stage I delamination is consistent with this process being electrochemically driven. The potential for stage I delamination depends on the swelling state of the gel ($\Phi_I = -3.8$ V for $H/h = 1.9$ vs −4.5 V for $H/h = 1.5$), indicating that electrochemical reduction alone is not sufficient to explain the phenomenon, but that the onset of debonding and buckling also depends on the level of compressive stress in the gel. (We note that the temperature to achieve $H/h = 1.5$ is also higher than that for $H/h = 1.9$ by ≈10 °C, but an increase in temperature would be expected to increase the electrochemical current at a given potential, which should facilitate delamination, whereas the opposite trend is seen.)

Stage II buckling is driven by formation of a gas bubble between the cathode surface and the gel, presumably as the pressure of dissolved hydrogen generated by electrolysis of water becomes sufficiently large to enable nucleation of a gas bubble. This assertion is substantiated by the dramatic growth in volume of the region between the bottom surface of the gel and the electrode (Figure 2d–f), which occurs on a time-scale that is too rapid to be explained by poroelastic transport of water across the gel thickness, as well as by the pronounced increase in optical contrast, and therefore refractive index difference (Figure 2b,c), from stage I to stage II blisters. Furthermore, the electrochemical current shows a second pronounced jump in the vicinity of stage II delamination (Figure S2, Supporting Information), suggesting that this process is driven by an increase in the rate of electrochemical hydrolysis. The critical potential was again found to depend on the swelling level of the gel ($\Phi_{II} = -4.6$ V for $H/h = 1.9$ vs −5.1 V for $H/h = 1.5$), suggesting that bubble nucleation is also coupled to the elastic energy of the gel.

We next turn to the origin of the distinct morphologies of the delamination blisters found in stage I and II. When the gel is initially delaminated from the electrode, it can buckle out-of-plane to relieve the compressive elastic stresses generated by confined swelling. However, it is not free to buckle into an arbitrary configuration, but is also instantaneously constrained to preserve its volume. Gradually, the gel may absorb water from the overlying aqueous medium and therefore increase in volume; water can also be transported across the gel and into the region between the gel and electrode. At long times, the gel should therefore be able to adopt an equilibrium configuration (while still bonded to the surrounding substrate regions), and the pressure within the fluid under the gel should equalize with that above the gel. We note that the importance of this volume constraint on buckling of soft membranes was invoked by Velankar and co-workers[28] to explain their similar observations, and was recently shown by Stone and co-workers to play

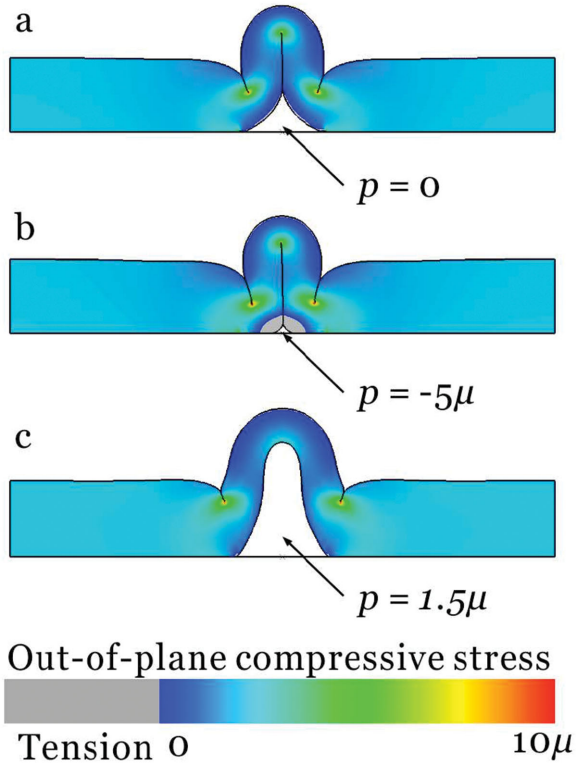

Figure 3. Buckling mechanism. a) The debonded gel buckles above the electrode upon swelling. There is significant out-of-plane compression near the tip of self-contact. b) When the gap between the debonded gel and the electrode has negative pressure relative to the bulk solution, the debonded gel may be tightly constrained against the electrode. c) When the gap between the debonded gel and the electrode has positive pressure relative to the bulk solution, the self-contact opens up. There is less out-of-plane compression near the top of the buckled gel.

an important role in the context of delamination buckling of lipid membranes.[58]

To shed additional light on the transition between stage I and stage II blisters, we performed finite element simulations using the commercial software package Abaqus. As a qualitative analysis, only a cross-section of the gel perpendicular to the electrode strip is simulated, and the deformation of the cross-section is constrained to plane strain condition. Since the gel layer is debonded from the electrode but bonded to the substrate elsewhere, the swelling causes the debonded gel to buckle up and form self-contacting regions, as shown in **Figure 3**a. Substantial out-of-plane compression is generated near the tip of the self-contact, which can drive the blister to buckle along the out-of-plane direction, i.e., to adopt a telephone-cord like morphology.

Note that the buckling of the debonded gel requires the diffusion of water into the gap between the debonded gel and the electrode. At the initial stage of the buckling, the diffusion of water may be much slower than the elastic deformation of the gel. The gap may thus be negatively pressurized relative to the bulk solution. In Figure 3b, it is shown that with a pressure of −5 μ in the gap, the debonded gel is tightly constrained against the electrode, leaving only a very small volume between the gel and the electrode. As the water gradually diffuses through the gel, the pressure difference between the gap and the bulk

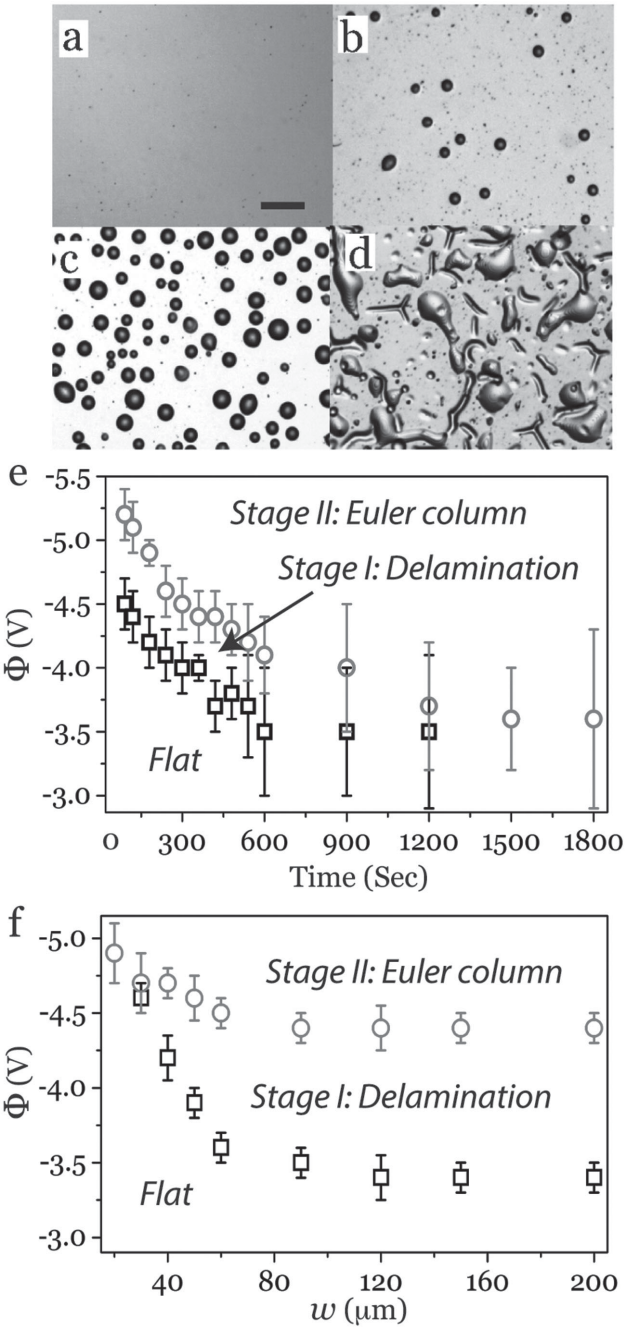

Figure 4. Effects of surface plasma treatment on gold electrodes and actuation voltages. Optical images of a planar gold electrode surface treated with O_2 plasma for times of a) 2 min, b) 4 min, c) 8 min, and d) 15 min show a progressive increase in the size and number of buckled features; the scale bar is 20 μm. e) The critical voltages Φ_I (squares) and Φ_{II} (circles) both decrease with increasing plasma treatment time. Parameters for this experiment are: $h = 25$ μm, $H = 45$ μm, $w = 60$ μm, $a = 90$ μm. f) The critical voltages Φ_I and Φ_{II} are plotted as a function of w, with $H/h = 1.8$ and $a/w = 2$.

solution eventually disappears and the equilibrium buckling in Figure 3a is obtained.

When gas is evolved from the electrode, the gap may be positively pressurized relative to the bulk solution. In Figure 3c, it is

shown that with a pressure of 1.5 μ, the self-contact opens up, leaving a large volume between the debonded gel and the electrode. The out-of-plane compressive stress is greatly released. In addition, the blister cross-section becomes wider. Both changes reduce the favorability of the serpentine morphology, contributing to the straight-sided morphology of stage II blistering.

As nucleation events are essential to determine the onset of both stages—nucleation of a debonded region in stage I, and of a gas bubble in stage II—it follows that the process ought to be highly sensitive to the presence of defects on the electrodes. Indeed, as summarized in **Figure 4**a–d, buckled features generated on the gold surface during oxygen plasma facilitated both steps. For increasing times of plasma exposure, the density and sizes of defects both increased (Figure S3, Supporting Information), coinciding with a reduction in magnitude of both Φ_{I} and Φ_{II} by more than 1 V (Figure 4e). For treatment times longer than ≈20 min, the initial delamination and bubble nucleation were simultaneous, leading to the direct formation of a straight-sided blister. Elsewhere in the paper, however, we fix the treatment time at 5 min or below, where defects are minimal and there is a clear separation between stage I and II.

As the onset of both stages also depends on the elastic energy of the gel, a dependence on the lateral electrode dimensions, and therefore the size of the debonded region, is to be expected. To evaluate this effect, samples on IDE substrates with w ranging from 20 to 200 μm were prepared, and delamination of gels with h = 25 μm was studied at a fixed swelling ratio of 1.8. As shown in Figure 4f, Φ_{I} exhibits a strong dependence on w, increasing in magnitude from −3.6 V for w = 60 μm, up to −4.2 V by w = 40 μm. Interestingly, Φ_{II} shows a much weaker dependence, beginning at ≈−4.7 V and increasing in magnitude by no more than 0.1–0.2 V over the same range. This suggests that bubble nucleation is less strongly coupled to the elastic energy of the gel than is debonding, which is also consistent with the smaller observed shift in Φ_{II} due to changes in swelling level, as described above. For values of w = 30 μm and below, no clear stage I buckling is observed; instead, debonding becomes coincident with bubble formation.

As summarized in **Figure 5**a, three basic morphologies were found for stage I blisters, depending on the degree of swelling of the gel layer: isolated blisters ($1.3 \le H/h \le 1.5$, Figure 5b), channeled but irregular blisters ($1.5 \le H/h \le 1.7$), and regular telephone cord blisters ($1.7 \le H/h \le 1.9$, Figure 5c). The normalized amplitude of these stage I features also increases with preswelling, from an average A/H = 1.53 at H/h = 1.3 to A/H = 2.31 at H/h = 1.9 (Figure 5d; h = 25 μm, w = 60 μm, a/w = 2). Stage II blisters show a similar trend, although are consistently slightly larger in amplitude (Figure 5d). Furthermore, the value of A for stage II blisters can be easily tuned by variations in the electrode width w (Figure 5d).

In addition to straight-sided Euler columns, it is also possible to achieve localized debonded blisters using a circular electrode geometry, as shown in Figure 5f,g (and Movie S2, Supporting Information). The gel surface locally debonds above the circular cathode to a stage I blister, and then inflates into a stage II blister with a spherical cap. With the voltage maintained, or switched off, the spherical bubble does not propagate down the straight portion of the electrode, but instead remains

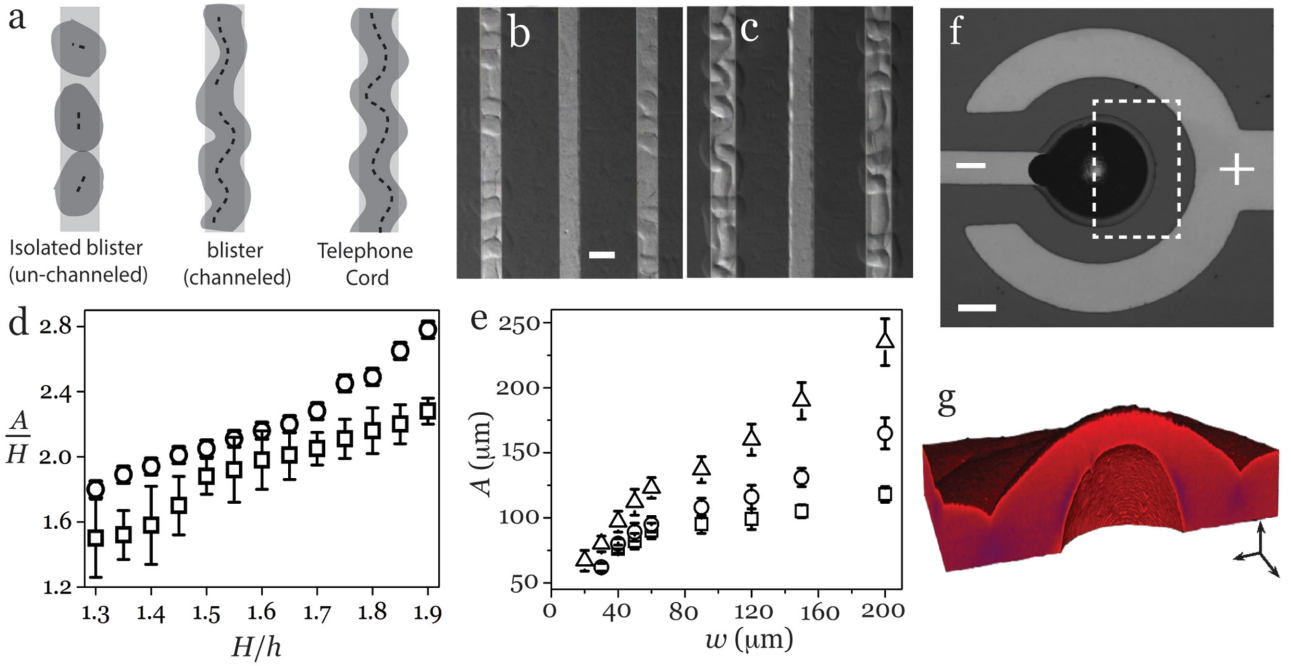

Figure 5. Structure of delamination blisters. a) Schematic illustration of stage | delamination as unchanneled isolated blisters (optical observation in panel (b), the scale bar is 50 μm), channeled blisters with (optical image in panel (c)), and telephone cord structures. (d) The normalized out-of-plane displacement for stage I (square) and stage II (circle) as function of the preswelling ratio, H/h. Parameters for this experiment are: h = 25 μm, w = 60 μm, a = 120 μm. e) The amplitude of stage II blisters increases with electrode width, as shown for H/h of 1.9 (triangle), 1.7 (circle), and 1.5 (square). f) An optical image and g) a 3D reconstruction from LSCM for a localized Euler blister on a circular electrode with diameter of 120 μm, the width of ring is 60 μm and the distance between the ring and central electrode is 60 μm.

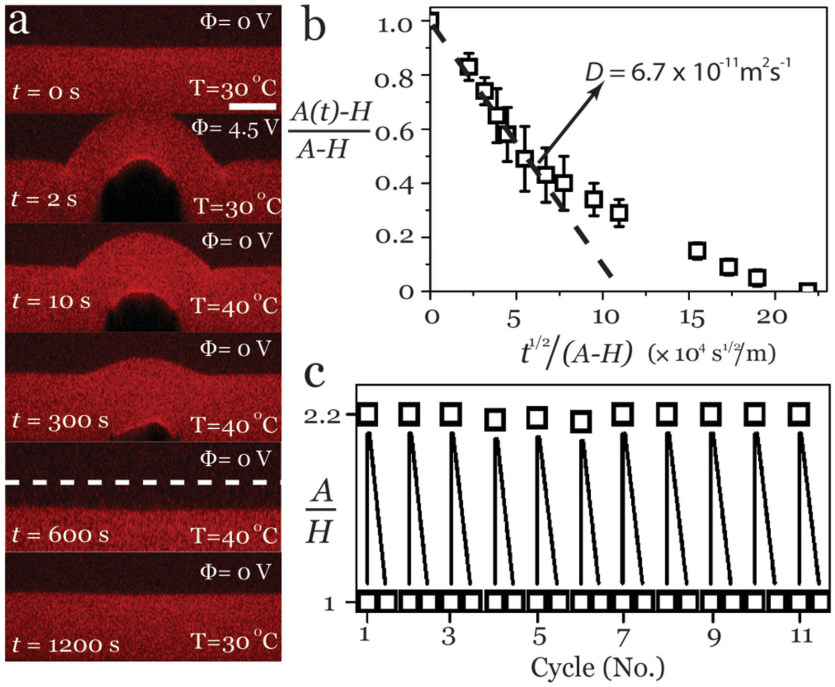

Figure 6. Temperature-induced recovery and cyclic actuation. a) A time series of LSCM cross-sections during an actuation-recovery cycle for a gel with $h = 25$ μm, preswelled to $H/h = 1.9$ at 30 °C, on an electrode with $w = 60$ μm. After electrochemically triggered stage II delamination, the sample is heated to 40 °C, causing it to deswell and return to the flat state, where it remains stably even after cooling back to 30 °C. The dashed line at $t = 600$ s indicates the initial thickness of preswollen gel. Scale bar: 20 μm. b) The normalized amplitude follows an apparently diffusive scaling at short times with a diffusion coefficient of 6.7×10^{-11} m^2 s^{-1} (slope of the dashed line). c) The normalized out-of-plane displacement of a single stage II blister shows good reproducibility over 11 cycles of actuation and recovery under a triggering voltage of 4.5 V.

stably located above the circular region. Such a device could potentially be used, e.g., as an adaptive valve in a microfluidic system, or a reconfigurable pixel in a tactile display.

Finally, we consider the possibility for cyclic actuation of delamination blisters by taking advantage of the deswelling of the thermally sensitive PNIPAM copolymer hydrogel. After driving stage II delamination and turning off the applied potential, a gel with initial thickness of $h = 25$ μm is heated to 40 °C. As shown in **Figure 6**a, the straight-sided buckle decreases in amplitude over a time-scale of ≈600 s, and the gel is eventually restored to a planar state. We characterize the rate of this process by a plot of the vertical deflection ratio $\frac{A(t)-H}{A-H}$ as $t^{1/2}/(A–H)$ (Figure 6b), where $A(t)$ is the deflection at time t. This plot shows an initially linear trend with a slope that yields a diffusion constant of $D = 6.7 \times 10^{-11}$ m^2 s^{-1}, which is similar in magnitude to that for poroelastic relaxation of these gels.[59] After the normalized amplitude has recovered to about half of its initial value, however, a break in the curve is seen and full recovery to the flat state proceeds more slowly. Importantly, when the gel is subsequently reswelled by cooling to 30 °C, no delamination is observed, indicating that the thiol groups remaining on the bottom surface of the gel after delamination are able to reestablish adhesion to the electrode surface. Repeated electrochemical delamination tests (Figure 6c) indicate good reproducibility over 11 cycles with a triggering voltage of 4.5 V, with no evident degradation or permanent delamination. Cyclic voltammetry measurements, performed about 20 min after recovery to the flat state, also reveal thiol reduction during each actuation cycle, further supporting the re-establishment of gold—thiol bonds (CV data are shown in Figure S4 in the Supporting Information for ten cycles). Although the magnitude of the reduction peak decreases over the first four cycles, it reaches nearly a steady-state value in subsequent cycles, indicating that a significant fraction of thiol groups can be reversibly reduced and reoxidized over multiple cycles.

3. Conclusion

In summary, we have described the two-stage electrochemically driven delamination buckling of hydrogel films supported on micropatterned interdigitated electrodes. Reductive desorption of the thiol adhesion-promoting layer, coupled with compressive swelling stresses in the film, drives delamination at a first critical potential into a tightly folded blister that exhibits secondary buckling into irregular or telephone-cord structures. At a second critical potential, electrolysis of water is sufficient to nucleate a bubble between the gel and the electrode surface, leading to rapid inflation of the blister into a straight-sided 'Euler column'. Both morphologies remain stable following the removal of the applied potential, although thermal deswelling of the gel can be used to restore the system to a planar and well-adhered state. We expect that the ability to controllably, reversibly, and rapidly drive delamination blistering of hydrogel films may find applications including as soft actuators, micro/nanofluidic devices, or surfaces with tunable properties.

4. Experimental Section

Microelectrode Fabrication and Surface Treatment: A silicon substrate covered with ≈100 nm of silicon oxide was cleaned using an ultrasonic bath (Branson 5510, 495 W, 40 kHz) with acetone for 15 min, followed by fabrication of Cr/Au electrodes (≈10 nm/≈100 nm thicknesses) by standard photolithographic patterning, e-beam evaporation, and lift-off in acetone. Patterned substrates were next cleaned in a Harrick Expanded Plasma Cleaner at 18 W and 300 mTorr (flowing oxygen) for a defined time period. After cooling the substrate to room temperature within a protection atmosphere of nitrogen, it was transferred to a beaker filled with 50 mL of toluene containing 4×10^{-3} M of bis(2-methacryloyl)oxyethyl disulfide (Sigma–Aldrich) and 25×10^{-3} M of 3-(methacryloxy)propyltrimethoxysilane (Gelest) for 12 h to coat the gold and silicon oxide regions, respectively, with adhesion-promoting layers.

Gelation and Device Assembly: Gelation of the aqueous based PNIPAM polymer was performed using a pregel solution with volume of 200 μL,

containing 825×10^{-3} M of *N*-isopropylacrylamide, 115×10^{-3} M of sodium acrylate, 4.5×10^{-3} M of *N*,*N*′-methylenebisacrylamide, and 5×10^{-3} M of rhodamine-B methacrylate. After mixing and degassing under 1 mTorr for 15 min, 0.3 µL of *N*,*N*,*N*′,*N*′-tetramethylethylenediamine and 1.0 µL of a 10 wt% aqueous ammonium persulfate solution were added. The mixture was loaded into a reaction chamber consisting of the anchoring substrate and a glass cover slip, separated by spacers (Kapton HN films, DuPont) to define the gel thickness (8, 13 or 25 µm). Gelation was completed in 30 min under the protection of a nitrogen atmosphere. Gel layers were rinsed with a phosphate buffer saline solution (Sigma–Aldrich) after disassembling the reaction chamber, and a testing chamber assembled using the gel covered substrate along with thicker (76 or 128 µm) Kapton spacers and a clean coverslip. The gap was filled with a phosphate buffer saline solution with an ionic strength of 150×10^{-3} M.

Electrical Actuation and Characterization: Gels were allowed to equilibrate for 10–30 min at the desired temperature prior to testing. Observation of delamination was conducted using an upright optical microscope (Zeiss Axiotech Vario) in brightfield reflection mode, or a Zeiss LSM 510 META laser scanning confocal fluorescence microscope, where a HeNe laser (wavelength 543 nm) was used to excite the rhodamine fluorophore (detection filter: 560 nm). The cyclic voltammetry measurements were carried out with a WaveNow USB Potentiostat (Pine Tech, US) at a scan rate of 20 mV s^{-1}. A TENMA DC power supply was used for applying the electric potentials. Experimental data processing and numerical analysis were performed using Zeiss LSM, ImageJ, Photoshop, and Matlab software.

Finite Element Simulations: Finite element simulations were conducted using the commercial simulation package – ABAQUS. The gel was modeled as an incompressible Neo-Hookean material model under plane-strain conditions, and the material was simulated in a cross-sectional plane perpendicular to the electrode strip. The gel layer was taken to be freestanding over the electrode, but bonded to the substrate elsewhere. The initial thickness of the gel was taken to be 0.3 of the width of the electrode. An isotropic, uniform expansion by 40% in volume was applied through thermal expansion to match the typical level of swelling in the experimental system, and the pressure in the region between the debonded gel and the electrode was controlled to mimic the effects of inflation of a gas bubble. The Explicit Dynamic solver was used in the simulation, and the static results were obtained after the kinetic energy was dissipated.

Supporting Information

Supporting Information is available from the Wiley Online Library or from the author.

Acknowledgements

The work at UMass was supported by the National Science Foundation through Grant No. DMR-1309331, and made use of facilities supported by NSF CMMI-1025020 and NSF BBS 8714235. The work at Harvard was supported by the NSF MRSEC (DMR 14-20570). Support for data analysis and manuscript preparation for BX at the University of Northumbria was provided by EPSRC and UoA 15 fund. The authors also thank REECE INNOVATION for helpful discussions.

Received: November 6, 2015
Revised: February 4, 2016
Published online: March 30, 2016

[1] M. D. Casper, A. O. Gozen, M. D. Dickey, J. Genzer, J.-P. Maria, *Soft Matter* **2013**, *9*, 7797.
[2] J. Yin, M. C. Boyce, *Nature* **2015**, *520*, 164.
[3] D. Chen, J. Yoon, D. Chandra, A. J. Crosby, R. C. Hayward, *J. Polym. Sci., Part B Polym. Phys.* **2014**, *52*, 1441.
[4] L. Ionov, *Langmuir* **2015**, *31*, 5015.
[5] J. Wang, B. Li, Y.-P. Cao, X.-Q. Feng, H. Gao, *Appl. Phys. Lett.* **2016**, *108*, 021903.
[6] D.-H. Kim, J. A. Rogers, *Adv. Mater.* **2008**, *20*, 4887.
[7] Y. Sun, W. M. Choi, H. Jiang, Y. Y. Huang, J. A. Rogers, *Nat. Nanotechnol.* **2006**, *1*, 201.
[8] S. P. Lacour, D. Chan, S. Wagner, T. Li, Z. Suo, *Appl. Phys. Lett.* **2006**, *88*, 204103.
[9] B. Xu, D. Chen, R. C. Hayward, *Adv. Mater.* **2014**, *26*, 4381.
[10] J. B. Kim, P. Kim, N. C. Pegard, S. J. Oh, C. R. Kagan, J. W. Fleischer, H. A. Stone, Y. L. Loo, *Nat. Photonics* **2012**, *6*, 327.
[11] T. Ohzono, H. Monobe, *Langmuir* **2010**, *26*, 6127.
[12] D. P. Holmes, B. Tavakol, G. Froehlicher, H. A. Stone, *Soft Matter* **2013**, *9*, 7049.
[13] J. Kim, J. Yoon, R. C. Hayward, *Nat. Mater.* **2010**, *9*, 159.
[14] E. P. Chan, E. J. Smith, R. C. Hayward, A. J. Crosby, *Adv. Mater.* **2008**, *20*, 711.
[15] P. C. Lin, S. Vajpayee, A. Jagota, C. Y. Hui, S. Yang, *Soft Matter* **2008**, *4*, 1830.
[16] S. G. Lee, D. Y. Lee, H. S. Lim, D. H. Lee, S. Lee, K. Cho, *Adv. Mater.* **2010**, *22*, 5013.
[17] K. Khare, J. Zhou, S. Yang, *Langmuir* **2009**, *25*, 12794.
[18] P. Görrn, M. Lehnhardt, W. Kowalsky, T. Riedl, S. Wagner, *Adv. Mater.* **2011**, *23*, 869.
[19] L. B. Freund, S. Suresh, *Thin Film Materials: Stress, Defect Formation and Surface Evolution*, Cambridge University Press, Cambridge, UK, **2003**.
[20] O. Borrero-Lopez, M. Hoffman, *Surf. Coat. Technol.* **2014**, *254*, 1.
[21] K. Zhang, M. Arroyo, *J. Appl. Phys.* **2013**, *113*, 193501.
[22] K. Zhang, M. Arroyo, *J. Mech. Phys. Solids* **2014**, *72*, 61.
[23] Z. Li, I. A. Kinloch, R. J. Young, K. S. Novoselov, G. Anagnostopoulos, J. Parthenios, C. Galiotis, K. Papagelis, C.-Y. Lu, L. Britnell, *ACS Nano* **2015**, *9*, 3917.
[24] M. S. Bronsgeest, N. Bendiab, S. Mathur, A. Kimouche, H. T. Johnson, J. Coraux, P. Pochet, *Nano Lett.* **2015**, *15*, 5098.
[25] C. Feng, Z. Yi, L. F. Dumée, C. J. Garvey, F. She, B. Lin, S. Lucas, J. Schütz, W. Gao, Z. Peng, L. Kong, *Carbon* **2015**, *93*, 878.
[26] S. Singamaneni, M. E. McConney, V. V. Tsukruk, *ACS Nano* **2010**, *4*, 2327.
[27] R. C. Hayward, B. F. Chmelka, E. J. Kramer, *Macromolecules* **2005**, *38*, 7768.
[28] S. S. Velankar, V. Lai, R. A. Vaia, *ACS Appl. Mater. Interfaces* **2012**, *4*, 24.
[29] Y. Ebata, A. B. Croll, A. J. Crosby, *Soft Matter* **2012**, *8*, 9086.
[30] J. S. Sharp, R. A. L. Jones, *Adv. Mater.* **2002**, *14*, 799.
[31] D. Vella, J. Bico, A. Boudaoud, B. Roman, P. M. Reis, *Proc. Natl. Acad. Sci. USA* **2009**, *106*, 10901.
[32] J. Rodríguez-Hernández, *Prog. Polym. Sci.* **2015**, *42*, 1.
[33] M. Asally, M. Kittisopikul, P. Rué, Y. Du, Z. Hu, T. Çağatay, A. B. Robinson, H. Lu, J. Garcia-Ojalvo, G. M. Süel, *Proc. Natl. Acad. Sci. USA* **2012**, *109*, 18891.
[34] J. N. Wilking, V. Zaburdaev, M. De Volder, R. Losick, M. P. Brenner, D. A. Weitz, *Proc. Natl. Acad. Sci. USA* **2013**, *110*, 848.
[35] Y.-S. Ryu, I.-H. Lee, J.-H. Suh, S. C. Park, S. Oh, L. R. Jordan, N. J. Wittenberg, S.-H. Oh, N. L. Jeon, B. Lee, A. N. Parikh, S.-D. Lee, *Nat. Commun.* **2014**, *5*, 4507.
[36] F. Zhou, W. T. S. Huck, *Phys. Chem. Chem. Phys.* **2006**, *8*, 3815.
[37] S. Xu, Z. Yan, K.-I. Jang, W. Huang, H. Fu, J. Kim, Z. Wei, M. Flavin, J. McCracken, R. Wang, A. Badea, Y. Liu, D. Xiao, G. Zhou, J. Lee, H. U. Chung, H. Cheng, W. Ren, A. Banks, X. Li, U. Paik, R. G. Nuzzo, Y. Huang, Y. Zhang, J. A. Rogers, *Science* **2015**, *347*, 154.
[38] J. Zang, S. Ryu, N. Pugno, Q. Wang, Q. Tu, M. J. Buehler, X. Zhao, *Nat. Mater.* **2013**, *12*, 321.

[39] L. Ionov, *Adv. Funct. Mater.* **2013**, *23*, 4555.
[40] O. Kuksenok, D. Deb, X. Yong, A. C. Balazs, *Mater. Today* **2014**, *17*, 486.
[41] M. A. C. Stuart, W. T. S. Huck, J. Genzer, M. Muller, C. Ober, M. Stamm, G. B. Sukhorukov, I. Szleifer, V. V. Tsukruk, M. Urban, F. Winnik, S. Zauscher, I. Luzinov, S. Minko, *Nat. Mater.* **2010**, *9*, 101.
[42] A. Döring, W. Birnbaum, D. Kuckling, *Chem. Soc. Rev.* **2013**, *42*, 7391.
[43] Z. Sun, Q. Huang, T. He, Z. Li, Y. Zhang, L. Yi, *ChemPhysChem* **2014**, *15*, 2421.
[44] L. Ionov, in *Intelligent Stimuli-Responsive Materials*, Vol. *1*, John Wiley & Sons, Inc., Hoboken, NJ, USA, **2013**.
[45] R. Kempaiah, Z. Nie, *J. Mater. Chem. B* **2014**, *2*, 2357.
[46] O. Kim, T. J. Shin, M. J. Park, *Nat. Commun.* **2013**, *4*, 2208.
[47] B. Xu, R. C. Hayward, *Adv. Mater.* **2013**, *25*, 5555.
[48] M. Tencer, P. Berini, *Langmuir* **2008**, *24*, 12097.
[49] S. Durocher, A. Rezaee, C. Hamm, C. Rangan, S. Mittler, B. Mutus, *J. Am. Chem. Soc.* **2009**, *131*, 2475.
[50] J. L. Shepherd, A. Kell, E. Chung, C. W. Sinclar, M. S. Workentin, D. Bizzotto, *J. Am. Chem. Soc.* **2004**, *126*, 8329.
[51] X. Jiang, R. Ferrigno, M. Mrksich, G. M. Whitesides, *J. Am. Chem. Soc.* **2003**, *125*, 2366.
[52] J. Ricka, T. Tanaka, *Macromolecules* **1984**, *17*, 2916.
[53] T. Tanaka, D. Fillmore, S. T. Sun, I. Nishio, G. Swislow, A. Shah, *Phys. Rev. Lett.* **1980**, *45*, 1636.
[54] H. Okuzaki, Y. Osada, *J. Biomater. Sci, Polym. Ed.* **1994**, *5*, 485.
[55] Y. Osada, J. P. Gong, *Prog. Polym. Sci.* **1993**, *18*, 187.
[56] M. W. Moon, H. M. Jensen, J. W. Hutchinson, K. H. Oh, A. G. Evans, *J. Mech. Phys. Solids* **2002**, *50*, 2355.
[57] J. W. Hutchinson, Z. Suo, in *Adv. Appl. Mech.* Vol. *29* (Eds: W. H. John, Y. W. Theodore), Elsevier, New York, NY, USA, **1991**.
[58] M. Staykova, M. Arroyo, M. Rahimi, H. A. Stone, *Phys. Rev. Lett.* **2013**, *110*, 028101.
[59] J. Yoon, J. Kim, R. C. Hayward, *Soft Matter* **2010**, *6*, 5807.